On the Design of Three-Layer Symmetric and Three-Layer Asymmetric Adherends in Lap Shear Joints

J. J. Radice
Mechanical Engineering Department
United States Naval Academy
590 Holloway Road, Annapolis, MD, 21402, USA
radice@usna.edu

J. R. Vinson
Department of Mechanical Engineering
University of Delaware
Spencer Laboratory, Newark, DE, 19717, USA
vinson@udel.edu

SUMMARY

Design studies are performed for composite material adherends in an axially loaded single lap shear joint with a three-layer adherend architecture. An optimal three-layer symmetric design and an improved three-layer asymmetric design are found. For the specific composite and adhesive material systems chosen, peel stresses are reduced by approximately 7% by using this improved three-layer asymmetric architecture.

Keywords: Joining of Advanced Composites, Structural Analysis and Optimization

INTRODUCTION AND LITERATURE SURVEY

Adhesive bonding offers an attractive alternative to the historically prevalent bolted/riveted approaches to joining load bearing elements. Bonded assemblies allow for a gradual transfer of load from one structural element to another. It also allows for the elimination of stress concentrations from drilled holes required for mechanical fastening. In their respective literature reviews, Vinson [1], Kuno [2], Hofer [3], Matthews [4], cite other benefits of bonded construction as: weight savings from thinner adherends, improved strength to weight ratios, improved fatigue life expectancies, isolation of vibrations, damping, accommodation of thermal expansion mismatches, accommodation of hygrothermal swelling, improved manufacturability, reduced tooling costs, reduced machining costs, improved aesthetic appearance, improved aerodynamic efficiency, and enhanced electrical insulation capabilities. The combination of performance advantages and analytical complexity has made adhesively bonded structures a fertile area of research with many analytical, finite element, and experimental studies having been offered over the years.

Efficient design begins with accurate analysis, but modeling even the simplest adhesively bonded joint is a formidable mathematical challenge. The analytical difficulties are quickly exacerbated by interesting facets such as: material anisotropy,

asymmetric material architectures, material non-homogeneity, and functional gradation over the length of the joint. It appears that a major tradeoff for the implementation of adhesively bonded composite material structures (other than economic) is mathematical complexity.

A large portion of the literature related to adhesively bonded composite structures deals with efforts to apply these distinctly "un-metallic" properties towards improving structural performance. In this spirit, Vinson and Xiao [5] and Mortensen and Thomsen [6] performed analyses of adhesively bonded single lap shear joints allowing for adherends with asymmetric architecture. Vinson [5] sought to use adherend asymmetry/bending-stretching coupling to reduce adherend lateral deflections and the resulting peel stress peaks. The analysis result supports this thesis, but it also cites a competing mechanism related to the reductions of tensile and bending stiffness resulting from asymmetric architecture. Neither of the above cited studies evaluated concrete candidate architectures and both of them invoked classical beam assumptions that neglect transverse shear deformation (making the adherends behave as though their transverse shear stiffness were infinite).

In an effort to further understand the influences of the various adherend stiffness moduli on adhesively bonded structures, Radice and Vinson [7] performed parametric studies of single lap shear joints. These studies confirmed the well known conclusion that peel stress increases dramatically from moderate reductions of adherend bending stiffness. The potential cited by Vinson [5] for peel stress reductions through bending-stretching coupling was also confirmed. Finally, it was observed that adherend peel stresses can be reduced through reductions of the adherend transverse shear stiffness. This latter conclusion appears to be unique and has interesting ramifications as will be seen later.

Based on the above studies, two interesting questions arise. Given that peel stresses are reduced by increasing adherend bending stiffness and decreasing adherend transverse shear stiffness, can one optimize a symmetric adherend to reduce peak peel stresses that would otherwise cause joint failure? What practical architectures can be devised to take advantage of the proposed benefits of bending-stretching coupling in concert with reduced transverse shear stiffness to reduce peak peel stresses?

The focus of the present work is the analysis, design, and evaluation of single lap shear joints including transverse shear deformation effects. The approach is to use the intuition gained from the investigations cited above to explore the design space for symmetric and asymmetric adherend concepts. The goal is to identify optimized three-layer symmetric and three-layer asymmetric architectures that result in reduced adhesive layer peel stresses in hope of improving joint strength.

SINGLE LAP SHEAR JOINT MODEL

Attention now turns to the modeling of axially loaded lap shear joints. The present studies are limited to the single lap shear joint geometry depicted in Figure 1.

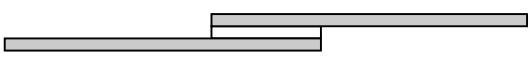

Figure 1: Single Lap Shear Joint

To capture elementary transverse shear behavior in the adherends, it is customary to assume that the axial (longitudinal) deformation is composed of a linear

superposition of neutral axis extension and cross sectional rotation. It is also typical to assume that through thickness strain/thickening of the structure can be neglected. These kinematic assumptions result in axial and lateral adherend deformations of following forms:

$$u(x,z) = u_0(x) + z\bar{\alpha}(x) \qquad w(x,z) = w(x) \tag{1,2}$$

Where u_0 is the neutral axis longitudinal deflection, $\bar{\alpha}$ is the cross sectional rotation, and w is the lateral deflection. These are not the only admissible kinematic assumptions for adherend deformation and the interested reader is referred to the comprehensive reference text by Reddy [8] for higher order deformation theories and/or layer-wise composite deformation theories. These high fidelity theories may provide fertile ground for further investigation.

Please consider the lap shear joints depicted in Figure 1. For such structures, each adherend has two distinct behavior regimes: one regime outside the adhesive bond line and another adjacent to the adhesive layer. Outside the adhesive bond line, the behavior changes gradually over the adherend length. However, adjacent to the adhesive layer, the deformation and stress states can have sharp gradients. Based on these observations, there are five distinct regions in a single lap shear joint: two adherend domains adjacent to the adhesive layer, two adherend domains outside the bond line area, and the adhesive layer itself. The simply supported, axially loaded single lap shear joint used in this study is presented in Figure 2.

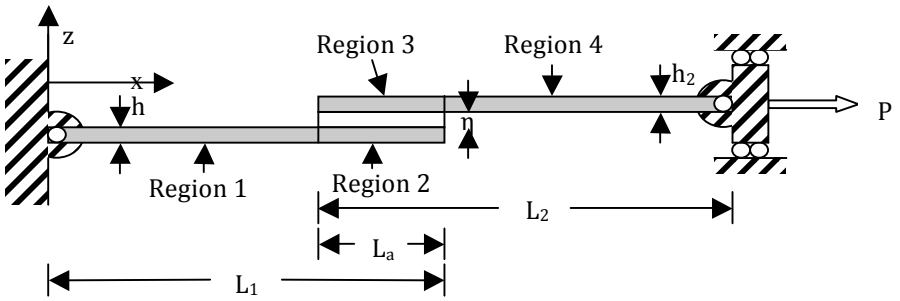

Figure 2: Lap Shear Joint Configuration

The key geometric parameters defined in Figure 2 are the adherend lengths (L_1, L_2), adherend thickness (h_1,h_2), adhesive/overlap length (L_a), adhesive layer thickness (η), and the externally applied axial load (P).

Each of the five regions in Figure 2 is to be treated as a separate structural element. Region 1 is asked to satisfy the global boundary conditions at the left end of the structure. Region 4 is asked to satisfy the global boundary conditions at the right end of the structure. The free edges of Region 2 and Region 3 are asked to be stress resultant and bending moment free. And the deformations are asked to be at least C^1 continuous across the interfaces of Regions 1 and 2 and Regions 3 and 4, respectively. The resulting boundary/interface conditions for this load case and geometry can be expressed as:

$$u_{o1}(0) = 0 \qquad w_1(0) = 0 \qquad u_{o1}(L_1 - L_a) = u_{o2}(L_1 - L_a) \qquad \bar{\alpha}_1(L_1 - L_a) = \bar{\alpha}_2(L_1 - L_a) \tag{3-6}$$

$$w_1(L_1 - L_a) = w_2(L_1 - L_a) \qquad \frac{\partial u_{o1}}{\partial x}(L_1 - L_a) = \frac{\partial u_{o2}}{\partial x}(L_1 - L_a) \qquad \frac{\partial \bar{\alpha}_1}{\partial x}(L_1 - L_a) = \frac{\partial \bar{\alpha}_2}{\partial x}(L_1 - L_a) \tag{7-9}$$

$$\frac{\partial w_1}{\partial x}(L_1 - L_a) = \frac{\partial w_2}{\partial x}(L_1 - L_a) \qquad \frac{\partial u_{o2}}{\partial x}(L_1) = 0 \qquad \frac{\partial \bar{\alpha}_2}{\partial x}(L_1) = 0 \qquad \frac{\partial w_2}{\partial x}(L_1) = -\bar{\alpha}_2(L_1) \tag{10-13}$$

$$\frac{\partial u_{o3}}{\partial x}(L_1 - L_a) = 0 \qquad \frac{\partial \bar{\alpha}_3}{\partial x}(L_1 - L) = 0 \qquad \frac{\partial w_3}{\partial x}(L_1 - L) = -\bar{\alpha}_3(L_1 - L) \qquad u_{o3}(L_1) = u_{o4}(L_1) \tag{14-17}$$

$$\bar{\alpha}_3(L_1) = \bar{\alpha}_4(L_1) \qquad w_3(L_1) = w_4(L_1) \qquad \frac{\partial u_{o3}}{\partial x}(L_1) = \frac{\partial u_{o4}}{\partial x}(L_1) \tag{18-20}$$

$$\frac{\partial \bar{\alpha}_3}{\partial x}(L_1) = \frac{\partial \bar{\alpha}_4}{\partial x}(L_1) \qquad \frac{\partial w_3}{\partial x}(L_1) = \frac{\partial w_4}{\partial x}(L_1) \qquad w_4(L_1 + L_2 - L_a) = 0 \tag{21-23}$$

Where the subscripts 1-4 correspond to regions 1-4 in Figure 2.

To model the adhesive layer, the commonly used Goland-Reissner model is invoked. The approach of this model is to try to capture the behavior of the adhesive layer as a continuum of through thickness tensile springs (for peel stress) and transverse shear springs (for shear stress) akin to an elastic foundation. The Goland-Reissner model also requires the assumption that the longitudinal tensile stresses (σ_{xx}) in the adhesive are negligible. The resulting adhesive stress element is defined in Figure 3.

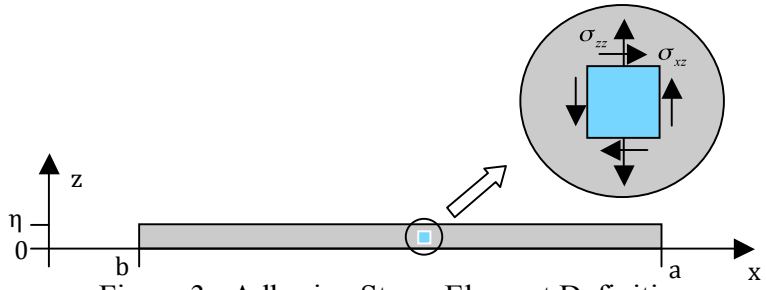

Figure 3: Adhesive Stress Element Definition.

The Goland-Reissner expressions for the peel stresses (σ_{zz}) and the shear stresses (σ_{xz}) take the following forms:

$$\sigma_{xz} = \frac{G_{adh}}{\eta}\left[\left(u_{o3} - \frac{h_2}{2}\bar{\alpha}_3\right) - \left(u_{o2} - \frac{h_1}{2}\bar{\alpha}_2\right)\right] \tag{24}$$

$$\sigma_{zz} = \frac{E_{adh}}{\eta}[w_3 - w_2] \tag{25}$$

Without derivation, using the above definitions for the adherend deflections and the adhesive layer stresses, the potential energy functional for this structure can be expressed as in [9]:

$$
\begin{aligned}
\Pi = & \int_{x=0}^{x=L_1-L_a} \left\{ \frac{A_{11,1}(x)}{2}\left(\frac{\partial u_{o1}}{\partial x}\right)^2 + B_{11,1}(x)\frac{\partial u_{o1}}{\partial x}\frac{\partial \bar{\alpha}_1}{\partial x} + \frac{D_{11,1}(x)}{2}\left(\frac{\partial \bar{\alpha}_1}{\partial x}\right)^2 + S_{55,1}(x)\left(\frac{\bar{\alpha}_1^2}{2} + \bar{\alpha}_1\frac{\partial w_{o1}}{\partial x} + \frac{1}{2}\left(\frac{\partial w_{o1}}{\partial x}\right)^2\right)\right\} dx \\
& + \int_{x=L_1-L_a}^{x=L_1} \left\{ \frac{A_{11,2}(x)}{2}\left(\frac{\partial u_{o2}}{\partial x}\right)^2 + B_{11,2}(x)\frac{\partial u_{o2}}{\partial x}\frac{\partial \bar{\alpha}_2}{\partial x} + \frac{D_{11,2}(x)}{2}\left(\frac{\partial \bar{\alpha}_2}{\partial x}\right)^2 + S_{55,2}(x)\left(\frac{\bar{\alpha}_2^2}{2} + \bar{\alpha}_2\frac{\partial w_{o2}}{\partial x} + \frac{1}{2}\left(\frac{\partial w_{o2}}{\partial x}\right)^2\right)\right\} dx \\
& \int_{x=L_1-L_a}^{x=L_1} \left\{ \frac{G_{adh}}{2\eta}\left[\left(u_{o3} - \frac{h_2}{2}\bar{\alpha}_3\right) - \left(u_{o2} - \frac{h_1}{2}\bar{\alpha}_2\right)\right]^2 + \frac{E_{adh}}{2\eta}\left[w_3 - w_2\right]^2 \right\} dx \\
& + \int_{x=L_1-L_a}^{x=L_1} \left\{ \frac{A_{11,3}(x)}{2}\left(\frac{\partial u_{o3}}{\partial x}\right)^2 + B_{11,3}(x)\frac{\partial u_{o3}}{\partial x}\frac{\partial \bar{\alpha}_3}{\partial x} + \frac{D_{11,3}(x)}{2}\left(\frac{\partial \bar{\alpha}_3}{\partial x}\right)^2 + S_{55,3}(x)\left(\frac{\bar{\alpha}_3^2}{2} + \bar{\alpha}_3\frac{\partial w_{o3}}{\partial x} + \frac{1}{2}\left(\frac{\partial w_{o3}}{\partial x}\right)^2\right)\right\} dx \\
& + \int_{x=L_1}^{x=L_1+L_2-L_a} \left\{ \frac{A_{11,4}(x)}{2}\left(\frac{\partial u_{o4}}{\partial x}\right)^2 + B_{11,4}(x)\frac{\partial u_{o4}}{\partial x}\frac{\partial \bar{\alpha}_4}{\partial x} + \frac{D_{11,4}(x)}{2}\left(\frac{\partial \bar{\alpha}_4}{\partial x}\right)^2 + S_{55,4}(x)\left(\frac{\bar{\alpha}_4^2}{2} + \bar{\alpha}_4\frac{\partial w_{o4}}{\partial x} + \frac{1}{2}\left(\frac{\partial w_{o4}}{\partial x}\right)^2\right)\right\} dx \\
& - P u_4\left(L_1 + L_2 - L_a\right)
\end{aligned}
\tag{26}
$$

The planar adherend stiffness quantities in (26) are the axial stiffness (A_{11}), bending-stretching coupling (B_{11}), and the bending stiffness (D_{11}). The transverse shear stiffness is designated here as S_{55} instead of the more common A_{55} nomenclature (as seen in the literature) to emphasize that this term is not a planar stiffness property. The definitions/expressions for these adherend stiffness terms are as they appear elsewhere in the literature, but to aid the reader in the design evaluations to follow, the expressions for these stiffness parameters are presented here for completeness:

$$A_{ij} = \sum_{k=1}^{N} \bar{Q}_{ij}\left[h_k - h_{k-1}\right] \qquad B_{ij} = \frac{1}{2}\sum_{k=1}^{N} \bar{Q}_{ij}\left[h_k^2 - h_{k-1}^2\right] \tag{27,28}$$

$$D_{ij} = \frac{1}{3}\sum_{k=1}^{N} \bar{Q}_{ij}\left[h_k^3 - h_{k-1}^3\right] \qquad S_{ij} = \frac{5}{4}\sum_{k=1}^{N} \bar{Q}_{ij}\left[h_k - h_{k-1} - \frac{4}{3h^2}\left[h_k{}^3 - h_{k-1}{}^3\right]\right] \tag{29,30}$$

The full expressions for the various lamina stiffness quantities, $\bar{Q}_{ij}$ are not useful for the present discussion and are thus omitted. It is sufficient for present purposes to simply note that the $\bar{Q}_{ij}$ terms are related to the various laminate tensile and shear moduli (E_{11}, E_{22}, G_{13}, G_{23}, etc…) The interested reader can find the full expressions in [8].

It is well known that a static system is in equilibrium when the potential energy a minimum. Analytical application of this concept results in Cauchy-Euler differential equations. For present purposes it is more convenient to commute the development and solution of Cauchy-Euler equations in favor of a Rayleigh-Ritz minimization of the potential energy functional. To this end, the adherend deflections are assumed to be polynomials with as-yet undetermined coefficients:

$$u_{0,m} = \sum_{n=0}^{\infty} a_{m,n}x^n \qquad \bar{\alpha}_m = \sum_{n=0}^{\infty} b_{m,n}x^n \qquad w_m = \sum_{n=0}^{\infty} c_{m,n}x^n \tag{31-33}$$

Where $a_{m,n}$, $b_{m,n}$, ,$c_{m,n}$ are the undetermined Rayleigh-Ritz Coefficients and m varies from 1 to 4 corresponding to Region 1 through Region 4 in Figure 2.

As usual, the Rayleigh-Ritz coefficients are obtained by substituting (31)–(33) into the potential energy functional (26), invoking the boundary/interface conditions (3)–(23), taking derivatives with respect to the arbitrary coefficients, and solving the resulting system of linear equations. For the high-order approximations used here (N=50+), this results in a system of 600+ equations on 600+ Rayleigh coefficients. The details of this solution are quite cumbersome, provide no insight into the system,

and are hence delegated to computer software. Attention now turns to the design studies that are of primary interest.

JOINT GEOMETRY AND MATERIAL PROPERTIES

The joint geometry, adhesive material, and adherend constituents are constant throughout these studies. This allows for the influence of adherend architecture to be investigated in isolation. The joint dimensions used here are specified in Table 1.

Table 1: Joint Dimensional Parameters

P	L_1	h_1	L_2	h_2	L_a	η
1 kN/in.	254mm	2.54mm	254mm	2.54mm	12.7mm	0.25mm

It is assumed that the reader has a working familiarity with the mechanics of orthotropic lamina as a detailed presentation of the underlying theory is beyond the scope of this paper. However, in the interest of clarity, the directional definitions for a unidirectional composite lamina is presented in Figure 4:

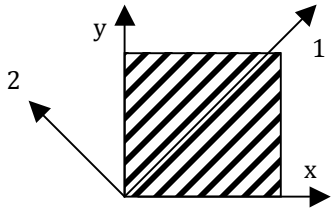

Figure 4: Orthotropic Lamina Direction Definitions

As seen in Figure 4, the "1" direction is down the fiber axis, the "2" direction is perpendicular to the fiber axis in the x-y plane, and the "3" direction is perpendicular to the x-y plane.

The adhesive used in this study is specified to be a common grade of epoxy. The adherends used in this study are specified to be a "garden variety" unidirectional carbon-epoxy composite material. Representative properties of such materials are presented in Table 2.

Table 2: Material Properties

E_{adh}	G_{adh}	E_{11}	E_{22}	G_{12}/G_{13}	G_{23}
4.75GPa	1.69 GPa	171.68 GPa	11.65 GPa	7.79 GPa	3.89 GPa

Unidirectional composite materials are known to demonstrate the extremes of composite material stiffness; the 0° (warp) stiffness and the 90° (weft) stiffness typically differ by an order of magnitude. The absence of lateral and transverse fibers also accentuates the difference between the various shear moduli. Specifically, unidirectional composites demonstrate a significant difference between the G_{12}/G_{13} and G_{23} shear moduli.

A laminate of composed of unidirectional composite materials potentially yields the maximum adherend bending stiffness (D_{11}), owing to the large warp direction stiffness (E_{11}). This has been demonstrated theoretically and experimentally to reduce adhesive peel stresses. The above cited directional stiffness discrepancy also potentially accentuates the bending-stretching coupling (B_{11}) in an asymmetric structure as

evidenced by the form of (28). Finally, the reduced G_{23} stiffness value allows for a reduction of the adherend transverse shear stiffness by placing plies oriented in the 90° (lateral) configuration near the adherend mid-plane.

In summary, the above cited "beneficial stiffness discrepancies" naturally reduce the design space to adherends composed solely of longitudinal (warp) and lateral (weft) fiber orientations. With this in mind, attention now turns to identifying an optimized symmetric adherend architecture.

OPTIMIZED SYMMETRIC ARCHITECTURE

To maximize the bending stiffness (D_{11}), the stiffest plies of a composite material should be as far from the adherend mid-plane as possible. For symmetric monocoque (non-sandwich structure) adherends, this implies that outermost plies should have longitudinal (0°) fibers. For maximum reduction of the adherend transverse shear stiffness (S_{55}), the plies closest to the adherend mid-plane should be laterally oriented (90°) to take advantage of the reduced shear stiffness, G_{23}. This information limits the adherend design space to the following generic architecture:

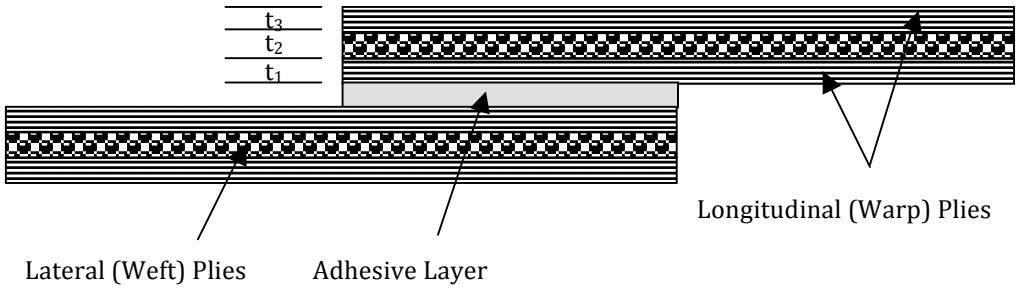

Figure 5: Generic Adherend Architecture

Where t_1, t_2, t_3 are the adherend ply thicknesses.

For each individual adherend to be symmetric, t_1 must be equal t_3. Since the two adherend thicknesses, h_1 and h_2, are specified to be the identical for the present study, they define a common adherend thickness, h. For monocoque adherends, these design space limitations result in a relationship between the ply thicknesses (t_1 and t_2) and the common adherend thickness (h):

$$2t_1 + t_2 = h \tag{34}$$

For the unfamiliar reader, an example of a typical peel stress profile is now presented. The present studies will use the all-warp fiber adherend configuration (t_2=0) with dimensions defined above in Table 1 as a basis for all subsequent comparisons. This is done primarily because this configuration represents the architecture which has the highest tensile, bending, and shear stiffness. This peel stress profile versus position in over the adhesive bond line length is presented in Figure 6.

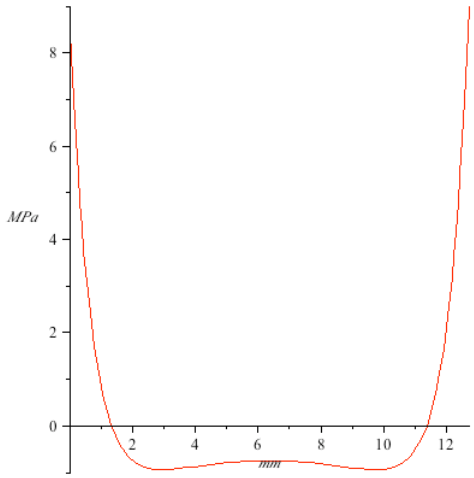

Figure 6: All-Warp Adherend Peel Stress Profile

Figure 6 is fairly typical of peel stress profiles for most single lap shear joints. Over much of the adhesive, the peel stresses are relatively small (compressive in this case). However, near the ends of the adhesive layer, the peel stresses peak sharply, reaching their maximum where the load begins to transfer between the adherend and the adhesive layer.

The peak value of the peel stress will, of course, depend on the specific geometry, material systems, and load considered. The present study seeks to identify an optimized three-layer symmetric architecture for the case specified in Table 1. If one is able to identify an optimum symmetric architecture for such an arbitrarily chosen case, then it suggests that such an optimized design can be found for any set of geometric parameters. To this end, the percent peak peel stress deviation from the all-warp baseline case (as seen in Figure 6) versus the transverse ply thickness (t_2) is presented in Figure 7.

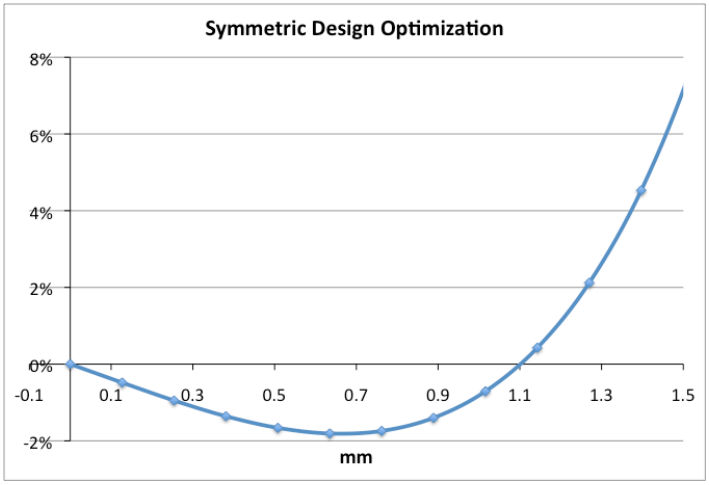

Figure 7: Percent Peel Stress Deviation vs. Transverse Ply Thickness

It is clear from Figure 7 there exists an optimum transverse ply thickness (t_2) in the vicinity of 0.7mm that reduces the peak peel stress approximately 2% below the all-warp fiber baseline. This implies that the benefits of adherend transverse shear stiffness reduction outpace the detriments of adherend bending stiffness reduction for this

optimized configuration. For the materials, geometries, and loads considered here, this transverse thickness comprises between 30% and 35% of the total adherend thickness.

However, one must be careful about what generalizations are made from this single result. For instance, no conclusion can be made regarding the percent peel stress reductions possible for arbitrary joint; 2% is for the current joint geometry only. Furthermore, no rule-of-thumb can be formulated as to what percentage of the adherend cross section should be composed of weft fibers to affect an optimal peel stress reduction; the 30% to 35% result applies to the current case only. However, it seems fair to postulate that there exists an optimal three-layer design that minimizes the adhesive peel stress for any arbitrarily specified joint lap joint configuration, even if t_2=0 is the optimum. An optimal design must be identified on a case-by-case basis. Attention can now turn towards an evaluation of asymmetric architectures in hopes of further reducing the adhesive peel stresses.

TWO-LAYER ASYMMETRIC ARCHITECTURE

In previous parametric studies it was identified that for an asymmetric architecture to reduce peel stresses the adherends must have their stiffest material on the side closest to the adhesive layer [7]. Orientation of the stiffest plies in this manner results in bending-stretching coupling (B_{11}) that tends to bend the structure towards the adhesive layer when subject to tensile loads. This is analogous to the bending of a bi-metallic strip towards the stiffer material when placed in tension. It can also be observed from the form of expression (28) the bending-stretching coupling (B_{11}) is maximized when one half of a monocoque structure's thickness is oriented with the warp direction down the length of the joint and the other half oriented perpendicular to the length. With these facts in mind, a two-layer asymmetric adherend architecture is proposed in Figure 8.

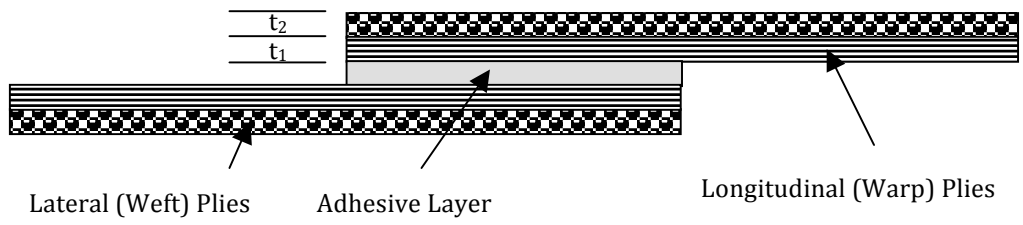

Figure 8: Two Layer Asymmetric Joint Architecture.

To evaluate the two-layer asymmetric architecture, a trade study of lateral layer ply thickness (t_2) versus percent peak peel stress deviation from the all-warp baseline case (as seen in Figure 6) is presented. As in the symmetric three-layer study, the adherends are prescribed to be of fixed thickness (h_1 and h_2). The results of this trade study are presented in Figure 9.

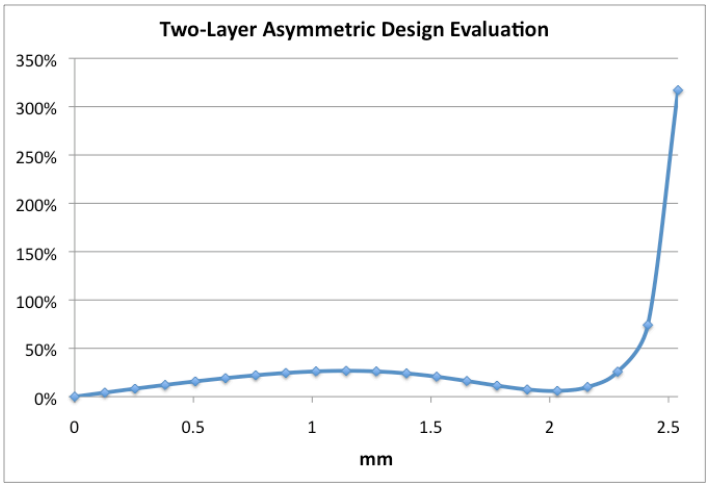

Figure 9: Two-Layer Asymmetric Design Evaluation

Figure 9 represents the full spectrum of lateral ply thickness. The lower extreme is the baseline case of all-warp fibers. The upper extreme represents the opposite case where adherend is composed entirely of 90° fibers. It is clear from this plot that the two-layer asymmetric architecture is, in fact, counterproductive in terms of it's effects on the adhesive layer peak peel stresses. This implies that the detriments of bending stiffness loss overwhelm the benefits of asymmetry. This was the concern cited by Vinson [5], and on prima facie, the failure of this design paradigm threatens to submarine the entire concept. To attempt to salvage the strategy, a three-layer asymmetric adherend architecture is proposed.

THREE-LAYER ASYMMETRIC ARCHITECTURE

To understand the rationale behind the three-layer design, it is useful to consider the design paradigms for some other applications. The two-layer composed of half warp fibers and half weft fibers maximizes the bending-stretching coupling (B_{11}). However, it appears that the bending stiffness reductions from such an architecture overwhelm the benefits of asymmetry. It is well known that having warp fibers as far as possible from the neutral axis of a beam or plate maximizes the bending stiffness; this approach motivates the use of sandwich structures composed of ultra-lightweight core materials encapsulated by stiff composite material face sheets.

This sandwich structure concept is the genesis of the so-called three-layer architecture. A two-layer asymmetric "core layer" is encapsulated by two warp layer "faces" to bolster the bending stiffness. Once the plies are consolidated together, this results in a three layer construction as illustrated in Figure 10.

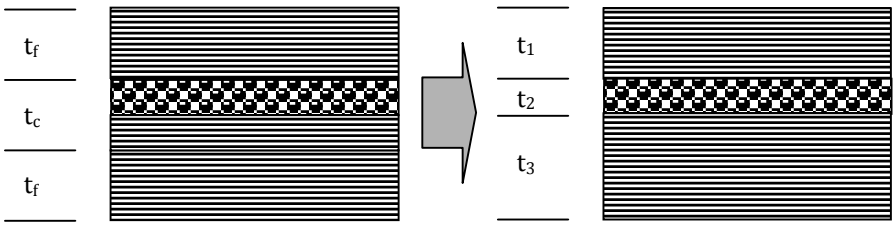

Figure 10: Three-Layer Asymmetric Architecture Composition

Where t_c is the "core" thickness, t_f is the "face" thickness, and t_1, t_2, and t_3 are defined as in Figure 5.

Given that the three layer thicknesses specified above must sum to the common adherend thickness, h, the three layer asymmetric architecture proposed above is a two

(unique) parameter design space. This manifests in a design space limitation on the ply thicknesses depicted in Figure 10:

$$t_1 + t_2 + t_3 = h \tag{35}$$

Exploration of this two parameter design space is an exercise of numerical experiments. Given the two parameter design space, the number of required experiments can be expected to go as the number of test increments squared. To expedite a preliminary evaluation of the three-layer asymmetric adherend concept, a further design space limitation is imposed based on the parametric study results from [7]: To maximize the bending-stretching coupling (B_{11}), the interface between the warp fibers and the weft fibers is constrained to be at the adherend mid-plane.

It can be seen from the form of (28) that equal stiffness plies equally spaced above and below the mid-plane yields a net-zero contribution to the bending-stretching coupling (B_{11}). Therefore, by placing the interface between t_2 and t_3 at the mid-plane, we maximize the resulting bending-stretching coupling. This approach has the ancillary benefit of having weft fibers close to the neural axis to reduce the adherend transverse shear stiffness. This logically motivated design space limitation yields the following relationships between the ply thicknesses:

$$t_1 = \frac{h}{2} \tag{36}$$

$$t_2 + t_3 = \frac{h}{2} \tag{37}$$

These limitations reduce the three-layer asymmetric architecture presented in Figure 10 to a one parameter design space. To evaluate the three-layer asymmetric architecture, a trade study of lateral layer ply thickness (t_2) versus percent peak peel stress deviation from the all-warp baseline case (as seen in Figure 6) is presented. As in the symmetric three-layer study, the adherends are prescribed to be of fixed thickness (h_1 and h_2). The results of this trade study are presented in Figure 11.

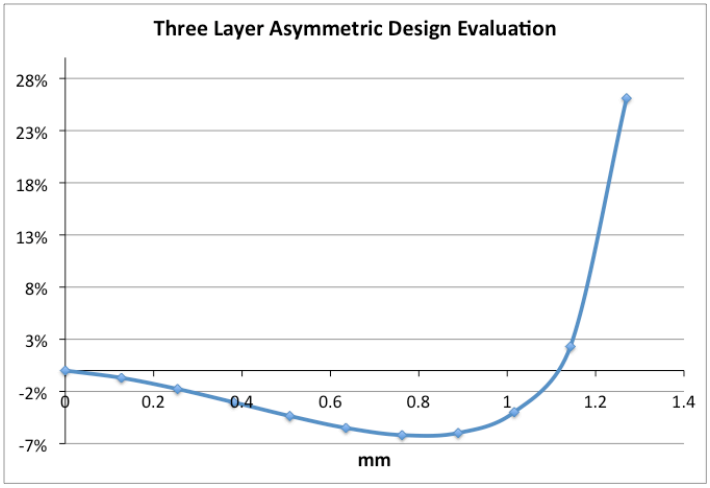

Figure 11: Three-Layer Asymmetric Architecture Evaluation.

It is clear from Figure 11 that an optima exists for the transverse ply thickness versus the percent peel stress deviation from the all-warp baseline case. One interpretation of this result is that the benefits of asymmetry are being realized for the

optimal case. without experiencing the full detriment of reduced bending stiffness. This is because the bending stiffness reductions are far less severe for the three-layer asymmetric architecture than the two-layer asymmetric approach via the placement of warp fibers on the outermost plies. For the loads and geometry considered, the transverse ply thickness is again in the vicinity of 30% of the total adherend thickness, but the peak peel stress reductions are nearly 7%.

As in the optimized three-layer symmetric architecture, one must be careful as to what conclusions are drawn from this single investigation. No definite conclusions can be drawn about what fraction of the cross section should be composed of transverse plies or what peak peel stress reductions can be expected. It is sufficient for present purposes to know that such improved asymmetric designs exist and can be identified.

CONCLUSIONS AND FUTURE WORK

A model of the single lap shear joint was developed including transverse shear deformation and the Goland-Reissner adhesive model. Using a Rayleigh-Ritz minimization of the potential energy functional, a high order approximation of all deformations, strains, and stresses for this system can be obtained.

Using this model and the conclusions of previously published works, an optimized symmetric adherend architecture for reduced adhesive peel stress was identified. This symmetric architecture takes advantage of the correlation between reduced adherend transverse shear stiffness and reduced peak peel stresses.

Subsequently, the joint model developed here was used to evaluate a two-layer asymmetric approach in an effort to take advantage of possible benefits of bending-stretching coupling. This two-layer approach was a dismal failure. However, from this failure arose the three-layer architecture that follows naturally from a combination of other successful design paradigms. Making a few design space limitations, the resulting three-layer asymmetric architecture demonstrated significant peak peel stress reductions.

There are two obvious areas where work can continue. First, the full design space for the three-layer architecture should be charted. This investigation will involve an exploration of the two parameter design space and the hundreds of numerical experiments that entails. Second, higher fidelity composite material kinematic assumptions can be explored. Higher fidelity modeling could yield results that more closely resemble the intricate complexities of real structures.

ACKOWLEGEMENTS

The author would like to thank Dr. Yapa Rajapakse of the Office of Naval Research for the agency's generous support of this research.

REFERENCES

1. J.R Vinson "Adhesive Bonding of Polymer Composites", Polymer Engineering and Science, 1989
2. J. K. Kuno, "Structural Adhesives and Bonding", Structural Adhesives and Bonding Conference, 1979

3. D. Kutcha and K.E. Hofer Jr. “Feasibility of Joining Advanced Composite Flight Vehicles”, 1969
4. Joining of Fibre-Reinforced Plastics. F.L. Matthews, Elsevier Applied Science,
5. J. R. Vinson and Shengkuan Xiao, “On the Use of Mid-plane Asymmetric Laminates for Adhesively Bonded Joints in Composite Structures”, 3rd Canadian Conference on Composite Materials, 2001
6. F. Mortensen and O.T. Thomsen, “Analysis of Adhesive Bonded Joints: A Unified Approach”, 2002
7. J. J. Radice and J. R. Vinson, “On the use of Quasi-Dynamic Modeling for Composite Material Structures: Analysis of Adhesively Bonded Joints with Mid-plane Asymmetry and Transverse Shear Deformation”, Composite Science and Technology, 2006
8. J.N. Reddy, Mechanics of Laminated Composite Plates and Shells, CRC.
9. Radice, J.J., Vinson, J.R., On the Analysis of Adhesively Bonded Structures: A High Order Semi-Elastic Adhesive Layer Model, Composites Science and Technology (2007)